Molecular Crystals and Liquid Crystals
Publication details, including instructions for authors and subscription information:
http://www.tandfonline.com/loi/gmcl16

Charge Carrier Mobility Measurements in Nematic Liquid Crystals

G. Derfel [a] & A. Lipiński [a]

[a] Technical University of Łódź, Institute of Physics, ul. Wólczańska 279, 93-005, Łódź, Poland

Version of record first published: 14 Oct 2011.

To cite this article: G. Derfel & A. Lipiński (1979): Charge Carrier Mobility Measurements in Nematic Liquid Crystals, Molecular Crystals and Liquid Crystals, 55:1, 89-100

To link to this article: http://dx.doi.org/10.1080/00268947908069793

Mol. Cryst. Liq. Cryst., 1979, Vol. 55, pp. 89–100
0026-8941/79/5501–0089$04.50/0

Printed in United States of America

Charge Carrier Mobility Measurements in Nematic Liquid Crystals

G. DERFEL and A. LIPIŃSKI

Technical University of Łódź, Institute of Physics, ul. Wólczańska 219, 93–005 Łódź, Poland

(*Received May 15, 1979*)

The nematic liquid crystal is considered as a weak electrolyte. The analysis of the time behaviour of the transient current flowing through the sample allows the estimation of the mean mobility of anions and cations. The electrohydrodynamic flows are avoided thanks to the application of low voltages. For *p*-octyloxyphenyl *p'*-pentyloxybenzoate the measured values of mobility are $\bar{\mu}_{\perp} = 0{,}9 \cdot 10^{-6}$ cm^2 V^{-1} s^{-1} and $\bar{\mu}_{\parallel} = 1{,}3 \cdot 10^{-6}$ cm^2 V^{-1} s^{-1} at 326K. The temperature behaviour of mobility and conductivity is described by identical activation energies: 0.48 eV and 0.16 eV in nematic and isotropic phase respectively.

INTRODUCTION

The problem of the exact measurement of the ions mobility in liquid crystals is still under consideration. There was a series of methods applied for this purpose. To our knowledge none of them gave the mobility of the single kind of ions non-assisted by electrohydrodynamic (EHD) flow. Table I lists the results of some experiments carried out by means of various methods.[1–15] Two main conclusions can be drawn from this review:

i) The results obtained by use of carriers generated by application of the voltage step method are generally higher than those obtained by other methods.

ii) There is only one paper reporting complete measurements of mobility non-assisted by EHD flows and its temperature behaviour.[8] It is also the only paper which gives a plausible confirmation of Walden's rule in its classical form, although the connection between mobility and viscosity

TABLE I

Review of mobility measurements results

Ref.	Material	Method	Mobility value (cm^2/Vs)	Temperature of measurement	EHD presence	Walden's rule validity
1	PAA	voltage pulse injection	$2.5 \cdot 10^{-4}$	?	yes	?
2	APAPA	voltage pulse injection	$3 \cdot 10^{-5}$	?	yes	?
3	PAA	ruby laser excitation	$4 \cdot 10^{-4}$	nematic, isotropic	?	$\mu\eta^a$ = const a = 1–1.5 (iso.) a = 4 (nem.)
		voltage pulse injection	$4–8 \cdot 10^{-4}$	nematic, isotropic	yes	no
4	MBBA	voltage pulse injection	$1.5–5 \cdot 10^{-6}$ voltage dependent	998 K	yes	no
5	PAA	voltage pulse injection	$3 \cdot 10^{-4}$	?	yes	?
6	MBBA	voltage pulse injection	$1.6 \cdot 10^{-5}$ (303 K)	nematic	yes	$\mu\eta^a$ = const a = 0.9–1.5
7	Merck 5 Merck 7a	voltage pulse injection	$1.2 \cdot 10^{-5}$ $1.3 \cdot 10^{-5}$ (293 K)	nematic	yes	$\mu\eta^a$ = const a = 1–1.3
8	MBBA	injection of holes photo-generated in Se	$6–9.4 \cdot 10^{-5}$	nematic	no	$\mu\eta$ = const
9	CBOA	polarity inversion	$10^{-7}–10^{-6} \cdot 10^{-5}$	smectic nematic	yes	?
10	BBOA	polarity inversion	$\mu_{\parallel} = 0.5–3 \cdot 10^{-6}$ $\mu_{\perp} = 3 \cdot 10^{-6}$	smectic, nematic, isotropic	?	?
11	chol. esters	polarity inversion	$10^{-7}–10^{-5}$	smectic, chol., isotropic	?	yes
12	MBBA (salt doped)	determination of equivalent conductance	$\bar{\mu}_{\parallel} = 2.47$ $\bar{\mu}_{\perp} = 1.86 \cdot 10^{-6}$	295.20 K	no	?

TABLE I (continued)

Ref.	Material	Method	Mobility value (cm^2/Vs)	Temperature of measurement	EHD presence	Walden's rule validity
13	MBBA (salt doped)	determination of equivalent conductance	$\bar{\mu}_{\parallel} = 0.7$ $\bar{\mu}_{\perp} = 0.43$ $\cdot 10^{-6}$	?	no	?
14	EPPH	determination of current relaxation time const.	$3.3 \cdot 10^{-6}$	397 K	no	?
15	MBBA	determination of current relaxation time const.	$9 \cdot 10^{-8}$	323 K	no	?
this work	nematic ester	determination of current relaxation time const.	$\bar{\mu}_{\parallel} = 1.3$ $\bar{\mu}_{\perp} = 0.9$ $\cdot 10^{-6}$ (326 K)	nematic, isotropic	no	?

PAA = *p*-azoxyanisole
APAPA = anisylidene-*p*-aminophenylacetate
MBBA = *p*-methoxybenzylidene *p*-*n*-butylaniline
CBOA = *p*-cyanobenzylidene-*p'*-octylaniline
BBOA = *p*-*n*-butoxybenzylidene-*p'*-octylaniline
EPPH = *p*(ethoxy-phenylazo)phenyl benzoate

seems unquestionable from other papers too. It is difficult therefore to generalize the experimental results. There is a necessity for continuation of the mobility investigations employing various methods.

The fact (i) is due to the arising of the electrohydrodynamic flows in the investigated samples under high d.c. voltages. A simple experiment shows it beyond a doubt. In this experiment the intensity of current flowing through the liquid crystal layer and the transmitted light intensity were measured simultaneously. The result is presented by the oscillogram in Figure 1 obtained for the nematic ester *p*-octyloxyphenyl *p'*-pentyloxybenzoate. This substance was synthetized in the Institute of Organic Chemistry of Technical University of Łódź. It is a nematic in the temperature range 325.3–357.5 K, and at 326 K it possesses negative dilectric anisotropy equal to -0.42 and conductivity $1.6 \cdot 10^{-11}\,\Omega^{-1}\,cm^{-1}$. It is evident that EHD instabilities, which induce the decrease of transparency because of dynamic scattering, arise earlier than the charge carriers reach the collecting electrode, which is manifested by the peak of the current. The same result was obtained for some other nematic liquid crystals e.g. for Merck 5 and Merck 7a, which were

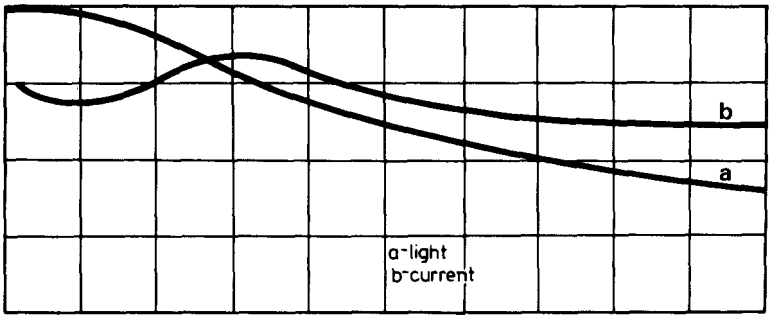

FIGURE 1 Time behaviour of current and light intensity, $U = 100$ V, $l = 50$ μm, $T = 325.5$ K. Horizontal scale: 10 ms/div.

the objects of mobility measurements reported earlier.[7] It points out that the use of methods with voltages lower than EHD threshold is required.

We applied such a method based on Gaspard, Briere, Herino and Mondon's papers.[15,16] These authors treated liquid crystals as weak electrolytes. In their experiment high voltage (up to 1500 V) was applied to 1 cm thick layer of MBBA in its isotropic phase. The injection phenomena leading to EHD motion were excluded by ion exchange membranes coated electrodes. The model considered in the paper cited above[16] assumes the existence of ions resulting in the dissociation process:

$$\begin{array}{ccc} AB & \underset{k_R}{\overset{k_D}{\rightleftharpoons}} & A^+ + B^- \\ v & & n^+ = n^- = n \end{array}$$

where k_D and k_R are the dissociation and recombination kinetic constants, v is the concentration of non-dissociated molecules and $n-$ the concentration of ions of every sign. At thermal equilibrium $n = (k_D v/k_R)^{1/2}$. When the electric field E is applied to the sample there flows the current whose density is time dependent and fulfills the equation:

$$\mathrm{d}i(t)/\mathrm{d}t = 2i_s/\tau_T - \tau_T i(t)^2/(2\tau_R)^2 2i_s - 2i(t)/\tau_T \tag{1}$$

where new constants are introduced:

The chemical relaxation time

$$\tau_R = \tfrac{1}{2}(k_R k_D v)^{-1/2} \tag{2}$$

The ionic mean transit time

$$\tau_T = 2l/E(\mu^+ + \mu^-) \tag{3}$$

The saturation current density

$$i_s = k_D vel \tag{4}$$

(here l is electrode spacing, μ^+ and μ^- are the mobilities of cations and anions respectively and e is the electron charge).

The exact solution of Eq. (1) has the form:

$$i(t) = 2i_s(2\tau_R/\tau_T)^2\left\{[1 + (\tau_T/2\tau_R)^2]^{1/2}\frac{1 + c\exp(-t/\tau')}{1 - c\exp(-t/\tau')} - 1\right\} \quad (5)$$

where

$$c = \frac{1 + (2\tau_R/\tau_T)\{1 - [1 + (\tau_T/2\tau_R)^2]^{1/2}\}}{1 + (2\tau_R/\tau_T)\{1 + [1 + (\tau_T/2\tau_R)^2]^{1/2}\}}$$

and

$$\tau' = (\tau_T/2)[1 + (\tau_T/2\tau_R)^2]^{-1/2}.$$

Briere, Herino and Mondon[15] used the simplification based on the relation $\tau_R \gg \tau_T$. Then the current density following the application of the field obeys the law:

$$i(t) = i_s[1 + (4\tau_R/\tau_T - 1)\exp(-2t/\tau_T)]. \quad (6)$$

The mean mobility can be therefore calculated from the time constant of the current changes.

It should be mentioned, however, that in spite of the complexity of the function Eq. (5) it can be well approximated by exponentially decreasing the function of type Eq. (6) in the wide range of τ_T/τ_R ratios but with the time constant lower than τ_T. The difference is about 15% when $\tau_R = \tau_T$, 4% when $\tau_R = 3\tau_T$ and 1.3% when $\tau_R = 10\tau_T$. It is therefore better to use the other property of function Eq. (5) which allows the determination of the mean transit time of ions:

$$i(0)/i'(0) = -\tau_T/2 \quad (7)$$

where $i'(0) = \mathrm{d}i(t)/\mathrm{d}t$ for $t = 0$. This relation was employed in the present work.

EXPERIMENTAL

The nematic liquid crystal ester mentioned above was contained in a cell constructed of two SnO_2 coated glasses separated by teflon foil 30–100 μm thick. The cell was mounted in the electric heater ensuring good temperature homogeneity in the sample. The temperature was measured with an accuracy of 0.1 K by a thermocouple. The magnetic field of 0.6 T was applied parallel to the plane of the sample, to align the liquid crystal homogeneously. The

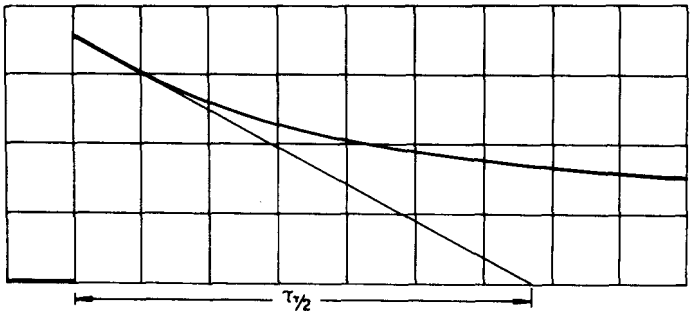

FIGURE 2 Current versus time curve for low voltage, $U = 3$ V, $l = 30$ μm, $T = 345.7$ K. Horizontal scale: 0.1 s/div. Geometrical interpretation of Eq. (7) is given.

aligning effect of the magnetic field was accordant to that of electric field and surface rubbing. Therefore, the perpendicular component of the mean mobility $\bar{\mu}_\perp = \frac{1}{2}(\mu_\perp^+ + \mu_\perp^-)$ was measured.

The current flowing through the sample after the application of the voltage step was a decreasing function of time. The applied voltages were generally lower than the threshold for EHD flow, but even 10 V were admissible because of long rise time of EHD phenomena. Figure 2 presents an example of experimental current *versus* time curve. Such curves obtained for various voltages and sample thicknesses possess properties predicted by Eq. (5):

i) The initial current I_0 was proportional to the voltage U and inversely proportional to the specimen thickness l:

$$I_0 \sim \frac{U}{l} \tag{8}$$

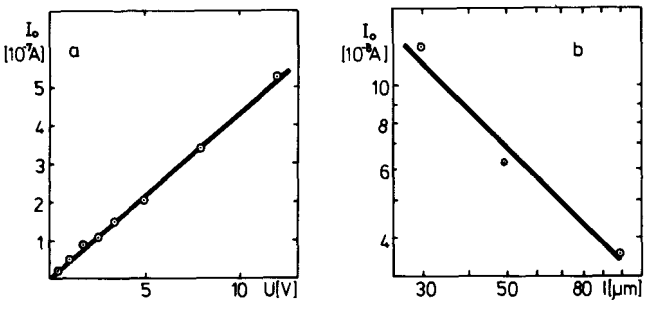

FIGURE 3 Initial current as function of voltage, $l = 30$ μm, $T = 341.6$ K (a), and thickness, $U = 3$ V, $T = 341.6$ K (b).

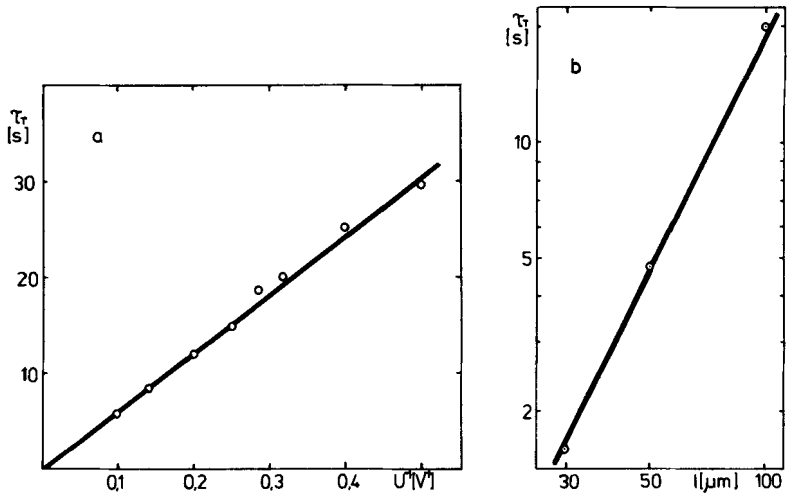

FIGURE 4 Mean transit time as function of reciprocal voltage, $l = 100\ \mu m$, $T = 340.1$ K (a), and thickness, $U = 3$ V, $T = 341.6$ K (b).

ii) The mean transit time calculated by means of Eq. (7) was proportional to the square of the thickness and inversely proportional to the voltage:

$$\tau_T \sim \frac{l^2}{U} \tag{9}$$

These relations are represented in Figures 3 and 4 respectively. From the slope of τ_T *versus* U^{-1} plot one can obtain the mean mobility. At the beginning of the mesophase, at 326 K, its value is $0.9 \cdot 10^{-6}$ cm^2 V^{-1} s^{-1}. The temperature dependence of mobility is given by Arrhenius' law, with activation energies 0.48 eV and 0.16 eV in nematic and isotropic phase, respectively. These values are equal to activation energies of conductivity (as well d.c. and a.c. one), see Figure 5. The measurement of conductivity in directions perpendicular and parallel to the director gave the anisotropy ratio of conductivity $\sigma_{\parallel}/\sigma_{\perp}$, which is plotted in Figure 6 as a function of temperature. It is equal to the mobility anisotropy $\bar{\mu}_{\parallel}/\bar{\mu}_{\perp}$.

The measured values of τ_T, I_0 and of the steady state current I_∞ allows a comparison in the shape of the current-time function predicted by Eq. (5) with an experimental curve. Figure 7 presents an example of such comparison, showing good agreement between experimental results and values $I(t)$ computed from Eq. (5) and by means of formulae for the initial and steady values of the current density:

$$i_0 = 4i_s\tau_R/\tau_T \tag{10}$$

$$i_\infty = i_0(2\tau_R/\tau_T)\{[1 + (\tau_T/2\tau_R)^2]^{1/2} - 1\} \tag{11}$$

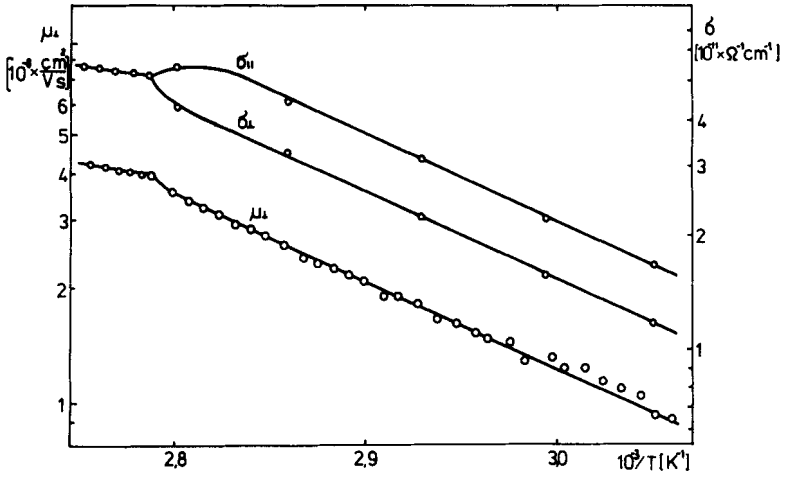

FIGURE 5 Temperature behaviour of mobility and conductivity.

This suggests that the model of the electrolyte is valid in the investigated samples.

The chemical relaxation time, τ_R, calculated from Eq. (11) was found to decrease with increasing voltage. The highest value of the τ_R/τ_T ratio obtained for most frequently applied voltages were about 2. This apparent voltage dependence of τ_R is related to the shape of the stationary current-voltage characteristic shown in Figure 8. This characteristic is therefore not described by Eq. (11) in which the electric field is included in the parameter τ_T.

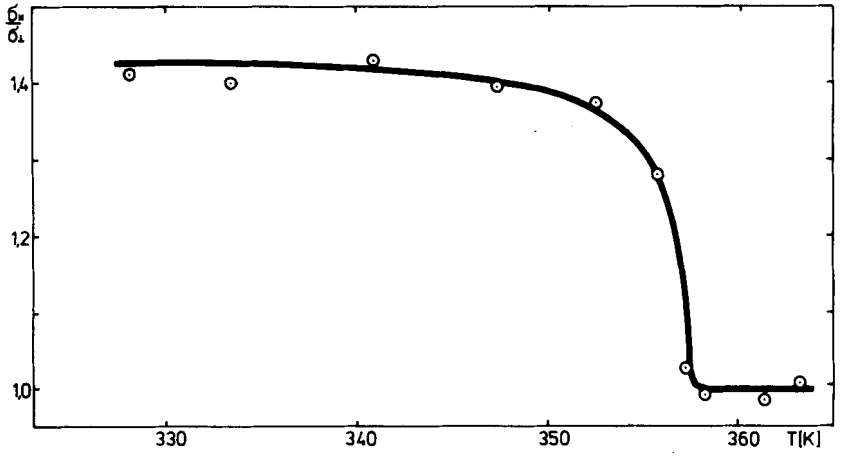

FIGURE 6 Conductivity and mobility anisotropy as function of temperature.

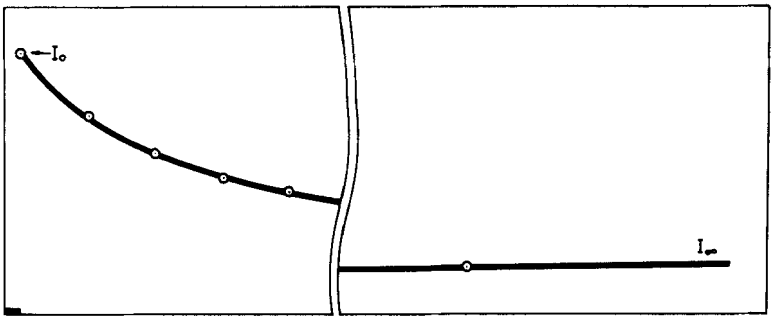

FIGURE 7 Comparison between theoretical (circles) and experimental (line) current-time functions, $U = 4$ V, $l = 50$ μm, $T = 335.7$ K.

The temperature behaviour of I_0, I_∞ and $\bar{\mu}$ is determined by identical values of the activation energy. It indicates that τ_R decreases with that activation energy because τ_R/τ_T remains constant. Charge carrier density remains constant too, so k_D/k_R is independent of temperature. Both kinetic constants k_D and k_R increase in the same way with the activation energy equal to that of the conductivity.

DISCUSSION

The method of ion-mobility measurement described above requires the determination of the slope of the tangent to the current-time curve in its initial point. It is possible to do that with a good accuracy thanks to the

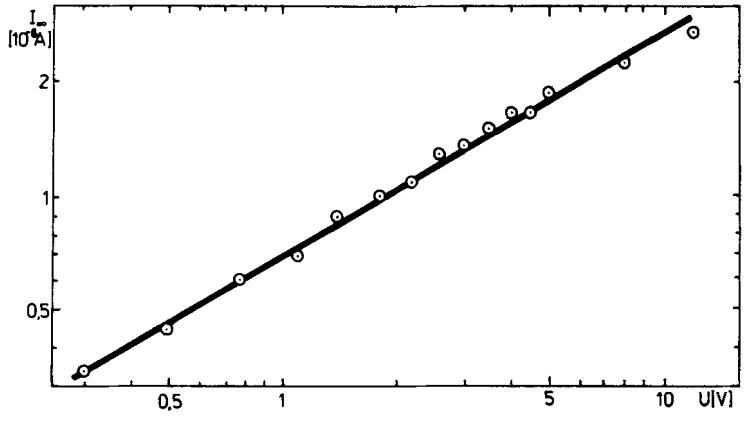

FIGURE 8 Stationary current-voltage characteristic, $l = 30$ μm, $T = 361.6$ K.

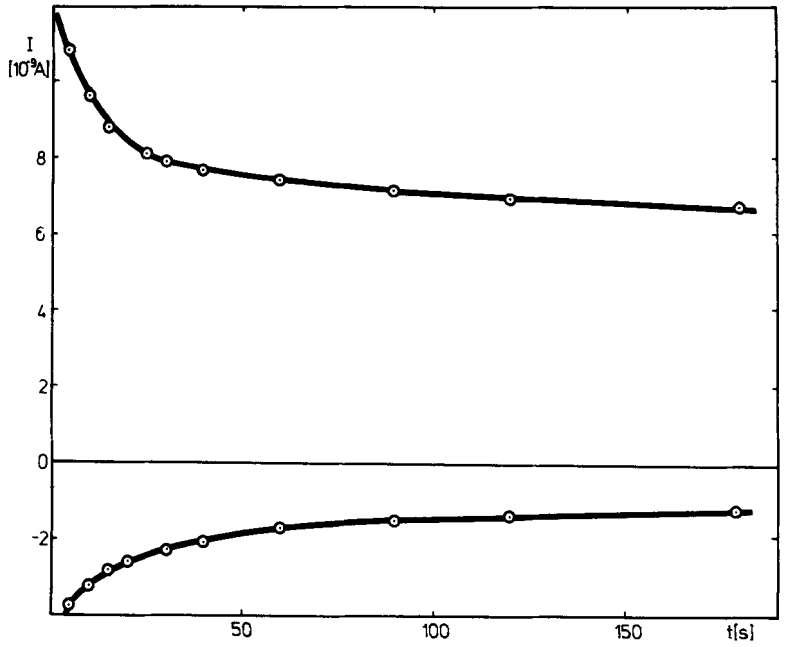

FIGURE 9 Current after application of voltage (upper curve) and reverse current (lower curve) as function of time, $U = 1.4$ V, $l = 30$ μm, $T = 341.9$ K.

negligibly small time constant of the circuit consisted of the sample capacitance and input resistance of the oscilloscope, as compared with the time constant of the measured current. Moreover, the time derivative of the current changes sufficiently slowly, so that the tangent can be easily drawn.

The decrease with time of the current follows well the theoretical predictions of Eq. (5) at least for t comparable with τ_T, whereas its voltage dependence does not agree with the theory. We suggest that this discrepancy can be due to the building up of the heterocharge near the electrodes. Two empirical facts support this hypothesis:

i) The current decreases noticeably even after time $t = 5\tau_T$;

ii) when the electric field is removed and the circuit is shortened a current flows in the opposite direction. Its intensity decreases for a long time. Figure 9 presents the example of the long-time current behaviour and of the reverse current.

The first effect can take place because the heterocharge for big t is high enough to decrease the effective electric field and the current. The second fact is due to slow decay of this heterocharge. The initial current, and with good accuracy the current during first τ_T period should not be disturbed by the

heterocharge. The current assumed as stationary (measured after about one minute) is smaller than the current not changed by the heterocharge. It results in too high and apparently voltage dependent values of τ_R. Nevertheless good agreement between experimental and theoretical current-time curve was found, since the shape of $i(t)$ function is weakly dependent on τ_R for t comparable with τ_T.

We conclude that this agreement and the results described by Eqs. (8) and (9) justify the acceptation of the weak electrolyte model and the application of its consequences to the mobility measurements.

Acknowledgments

The authors wish to thank Dr. A. Kuś and Dr. J. Wasiak for preparation of the investigated substance.

References

1. G. H. Heilmeier and P. M. Heyman, *Phys. Rev. Lett.*, **18**, 583 (1967).
2. G. H. Heilmeier, L. A. Zanoni, and L. A. Burton, *Proc. IEEE*, **56**, 1162 (1968).
3. K. Yoshino, S. Hisamitsu, and Y. Inuishi, *J. Phys. Soc. Japan*, **32**, 867 (1972).
4. J.-C. Lacroix and R. Tobazeon, *C. R. Acad. Sci. Paris*, **278B**, 623 (1974).
5. S. Hisamitsu, K. Yoshino, and Y. Inuishi, *Technol. Rep. Osaka Univ.*, **1045**, 201 (1971).
6. T. Yanagisawa, H. Matsumoto, and K. Yahagi, *Japan. J. Appl. Phys.*, **16**, 45 (1977).
7. A. Lipiński, W. Mycielski, and G. Derfel, *Mol. Cryst. Liq. Cryst. Lett.*, **41**, 137 (1978).
8. M. Yamashita and Y. Amemiya, *Japan. J. Appl. Phys.*, **17**, 1513 (1978).
9. K. Yoshino, K. Yamashiro, and Y. Inuishi, *Japan. J. Appl. Phys.*, **14**, 216 (1975).
10. K. Yoshino, N. Tanaka, and Y. Inuishi, *Japan. J. Appl. Phys.*, **15**, 735 (1976).
11. K. Yoshino, K. Yamashiro, and Y. Inuishi, *Japan. J. Appl. Phys.*, **13**, 1471 (1974).
12. R. Chang and J. M. Richardson, *Mol. Cryst. Liq. Cryst.*, **28**, 189 (1974).
13. G. J. Sprokel, *Mol. Cryst. Liq. Cryst.*, **26**, 45 (1974).
14. G. Briere, F. Gaspard, and R. Herino, *Chem. Phys. Lett.*, **9**, 285 (1971).
15. G. Briere, R. Herino, and F. Mondon, *Mol. Cryst. Liq. Cryst.*, **19**, 157 (1972).
16. G. Briere, F. Gaspard, and R. Herino, *J. Chim. Phys.*, **68**, 845 (1971).